

# Formation and size control of a Ni cluster by plasma gas condensation

Takehiko Hihara<sup>a)</sup> and Kenji Sumiyama

*Institute for Materials Research, Tohoku University, Sendai 980-8577 Japan,  
and CREST, Japan Science and Technology Corporation (JST) Japan*

(Received 13 May 1998; accepted for publication 24 July 1998)

We have constructed a plasma-gas-condensation type cluster deposition apparatus and tried to find the optimum operation conditions for controlling the cluster size. Transmission electron microscope (TEM) observation has been done to evaluate sizes of Ni clusters produced when varying the volume of a cluster growth region, sputtering power, and inert gas pressure. The mean cluster size decreases by decreasing the volume of growth region and the sputtering power. The smallest cluster obtained in this work is about 2.3 nm in diameter. We have considered the following two models for the cluster growth: (1) a cluster-cluster collision growth and (2) an atomic vapor condensation growth. The cluster growth speed estimated from the former is too slow, while that from the latter is reasonable in comparison with the present experiments. When stable embryos are made from atom collisions, they grow up faster and the final cluster sizes estimated from the latter model are consistent with those observed by TEM. © 1998 American Institute of Physics. [S0021-8979(98)01321-8]

## I. INTRODUCTION

Studies on nanometric metal and semiconductor clusters have been motivated by their unique physical and chemical properties (different from those of the bulk solids). Several experimental techniques have been applied to generate and characterize small particles and clusters.<sup>1-3</sup> Improvement and development of these cluster sources have been strongly desired for narrower cluster size distribution and more intensive cluster beam. Accordingly, we need a universal concept to realize the cluster formation process. A plasma-gas-condensation (PGC) type cluster source,<sup>4-8</sup> which is a combination of sputtering vaporization and inert gas condensation techniques, is one of the candidates for this purpose. It is versatile enough to vaporize transition metals and refractive elements and is able to control the cluster size by adjusting the sputter yield, the gas pressure, and the volume of the cluster growth region.

In previous reports,<sup>7,8</sup> we described nanometric Cr and Co clusters prepared by the PGC type cluster source and the effects of the sorts, pressure, and the flow rate of inert gases on the cluster formation. As the Ar gas flow rate increases, larger-sized clusters are produced. He gas is important to reduce the cluster size and its dispersion. The mean cluster size was between 6 and 13 nm.

In order to obtain smaller-sized clusters and to optimize the operation conditions of PGC, we summarize a guideline of fine particle formation by gas condensation.<sup>9</sup> At the initial stage of cluster nucleation, a three-body collision is necessary in the gas phase to release the latent heat of condensation,  $\Delta E_{lh}$ , for conserving the energy and momentum of the total system. When the cluster becomes large enough to transfer  $\Delta E_{lh}$  to its various internal degrees of freedom, two-body collisions become the main channels for the cluster

growth. Molecular dynamics and Monte Carlo simulations have indicated that this transition is expected to occur at the cluster containing about 7 atoms,<sup>10</sup> which is called an embryo. Once the embryo is stabilized, the cluster may further grow via the following procedures proposed within kinetic theory of the ideal gas:<sup>11,12</sup> a cluster-cluster collision and an atomic vapor condensation.

In this context, we have constructed another PGC type cluster beam deposition apparatus, in which the volume of a cluster growth chamber is variable. This article deals with the size variation of Ni clusters produced by the PGC apparatus when changing the operational parameters such as sputtering power, pressure in the growth chamber, and its volume. We then discuss the cluster growth mechanism in terms of the two models mentioned above.

## II. PLASMA-GAS-CONDENSATION CLUSTER SOURCE

### A. Overview

Figure 1 shows a schematic diagram of the present PGC apparatus. The metal vapors are generated by dc magnetron sputtering. A continuous Ar gas stream adjusted by a mass flow controller is injected in front of a sputtering target. Clusters nucleate in a high pressure Ar gas atmosphere,  $P_{Ar}=0.1-0.4$  kPa, and grow up in the space between the target,  $T_A$ , and the nozzle,  $N_1$  (the growth region). The length between  $T_A$  and  $N_1$ ,  $L_g$ , can vary by moving the sputtering source back and forth. He gas is also introduced into the sputtering chamber from the backside of the source to obtain smaller clusters.<sup>8</sup> The cluster beam is extracted through the  $N_1$  nozzle (5 mm in diameter) by differential pumping, where we used a powerful mechanical buster pump whose exhausting speed is 1200 m<sup>3</sup>/h under the present condition. The cluster beam is further collimated by the three skimmers,  $N_2$ ,  $N_3$ , and  $N_4$ , whose diameters are 5 mm. The

<sup>a)</sup>Electronic mail: Hihara@snap8.imr.tohoku.ac.jp

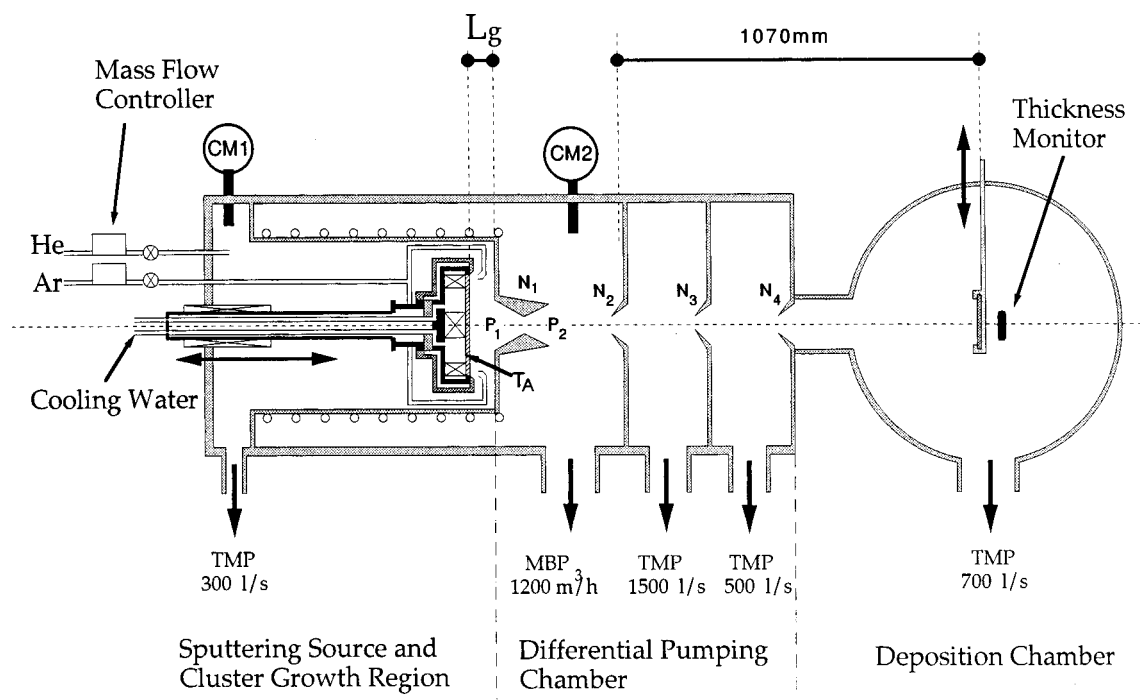


FIG. 1. Schematic diagram of plasma-gas-condensation (PGC) type cluster deposition apparatus. CM1, CM2: capacitance manometers. TMP: turbomolecular pump. MBP: mechanical buster pump.  $T_A$ : sputtering target.

background pressure of  $4 \times 10^{-7}$  Pa is attained in the deposition chamber by three turbomolecular pumps. During operation, the pressure of the deposition chamber is typically  $2 \times 10^{-5}$  Pa.

The microgrid, which was a carbon-coated colodion film supported by a Cu grid, was used as a substrate for transmission electron microscope (TEM) observation. The Ni clusters were deposited at room temperature. The deposition rate was measured by a quartz thickness monitor. The samples were transported through air and TEM observation was performed with a Hitachi HF-2000 electron microscope, operating at 200 kV.

## B. Gas dynamics

The pressure in the growth region,  $P_1$ , and the next room after the  $N_1$  nozzle,  $P_2$ , are measured by capacitance manometers, CM1 and CM2 as indicated in Fig. 1. Figure 2 shows  $P_1$  and  $P_2$  as a function of the total gas flow rate,  $V_T$ , with the different Ar and He gas flow rates  $V_{Ar}$  and  $V_{He}$ , during the operation.

The mass flow rate,  $\dot{m}$ , through the nozzle can be formulated by the following equation within the standard gas dynamics,<sup>13</sup> because the backpressure,  $P_2$ , is much smaller than the critical pressure,  $P^* = P_1 [2/(\gamma + 1)]^{1/(\gamma - 1)}$ :

$$\dot{m} = \frac{A_n P_1}{\sqrt{k_B T_1}} \sqrt{\gamma m \left( \frac{2}{\gamma + 1} \right)^{(\gamma + 1)/(\gamma - 1)}}, \quad (1)$$

where  $k_B$  is the Boltzmann constant,  $T_1$  is the temperature in the growth region,  $A_n$  is the cross section of the  $N_1$  nozzle, and  $\gamma = 5/3$  is the ratio of molar heat capacity for the monoatomic He and Ar gases. When the partial pressure of Ar in the growth region,  $P_{Ar} = 130$  Pa at  $V_{Ar} = 1.5 \times 10^{-4}$  mol/s

and that of He,  $P_{He} = 150$  Pa at  $V_{He} = 4.5 \times 10^{-4}$  mol/s (see Fig. 2), for instance, we obtain  $\dot{m} = 1.9 \times 10^{-4}$  mol/s for Ar and  $6.9 \times 10^{-4}$  mol/s for He gas from Eq. (1) with  $T_1 = 300$  K and  $A_n = 2.0 \times 10^{-5}$  m<sup>2</sup>. The estimated  $\dot{m}$  values are roughly in agreement with  $V_{Ar}$  and  $V_{He}$ , suggesting that the gas dynamics through the nozzle is isentropic. The drift velocity of the gas and cluster in the growth region,  $v_z$ , can be estimated to be about 0.4 m/s by the following equation:

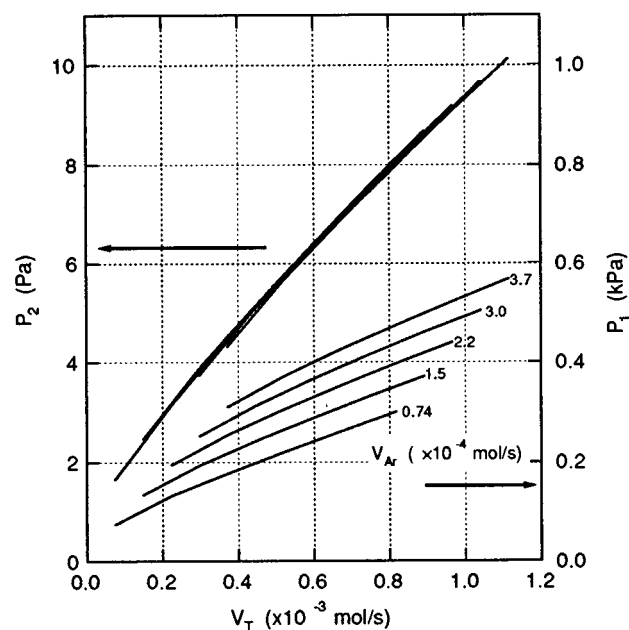


FIG. 2. Inert gas pressure in cluster growth region,  $P_1$ , and the first differential pumping chamber after nozzle,  $P_2$ , as a function of total gas flow,  $V_T = V_{Ar} + V_{He}$ .

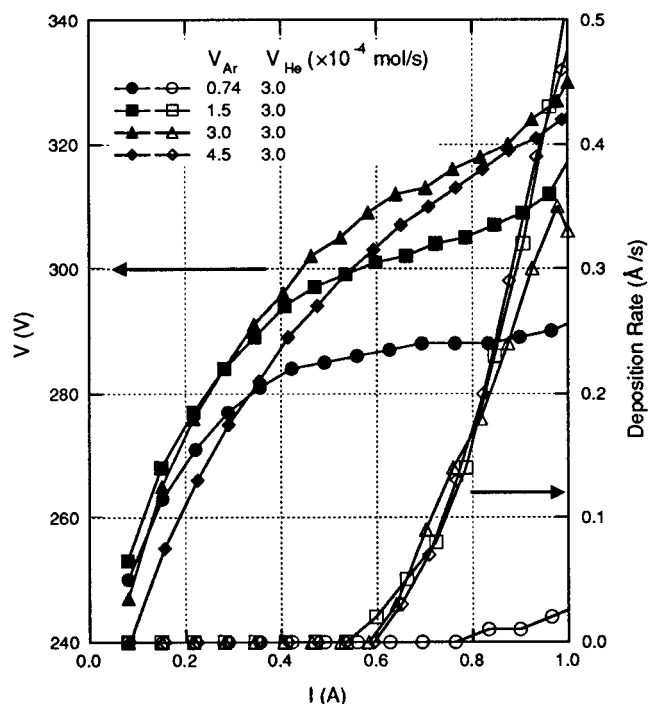


FIG. 3. Typical  $I$ - $V$  curves of sputtering source and cluster deposition rate with different Ar gas flows,  $V_{Ar}$ , and constant He gas flow.

$$\nu_z = \frac{mk_B T_1}{mA_g P_1}, \quad (2)$$

where  $A_g$  is the cross section of cluster growth region ( $1.4 \times 10^{-2} \text{ m}^2$ ).

### III. RESULTS

Figure 3 shows the dc voltage,  $V$ , applied on the Ni target (in the left axis) and a deposition rate of clusters on the substrate (in the right axis) as a function of the electrical current,  $I$ , between the target and the ground. The voltage is only moderately sensitive to the current between 0.4 and 0.8 A for  $V_{Ar} = 7.4 \times 10^{-5} - 1.5 \times 10^{-4} \text{ mol/s}$ . This is a typical behavior for magnetron sputtering. Magnetic fields formed beyond the target induces a magnetron motion of electrons in plasma, accelerating ionization of Ar gas above the critical voltage. This voltage plateau disappears for  $V_{Ar} > 3.0 \times 10^{-4} \text{ mol/s}$ . The mean free path of electrons in the plasma becomes short at high  $P_{Ar}$ , so that the ionization efficiency of Ar is not enhanced further.

With the low Ar flow,  $V_{Ar} = 7.4 \times 10^{-5} \text{ mol/s}$ , the deposition rate is one order lower than the others. The embryo formation and cluster growth are suppressed because the pressure in the growth region is not enough to thermalize Ni vapor. The clusters can be observed for  $V_{Ar} > 1.5 \times 10^{-4}$  and  $V_{He} > 3.0 \times 10^{-4} \text{ mol/s}$  as shown in Fig. 4. The cluster size increases with increasing electrical current,  $I$ , as shown in the insets of Fig. 4. The average cluster size is 3.6 nm for  $I = 1.0 \text{ A}$ , while it is 2.3 nm for  $I = 0.66 \text{ A}$ , where we investigated the deposition area of  $0.016 \mu\text{m}^2$ .

Figure 5 shows the cluster deposition rate as a function of the growth region length,  $L_g$ , at  $V_{Ar} = 1.5 \times 10^{-4}$  and

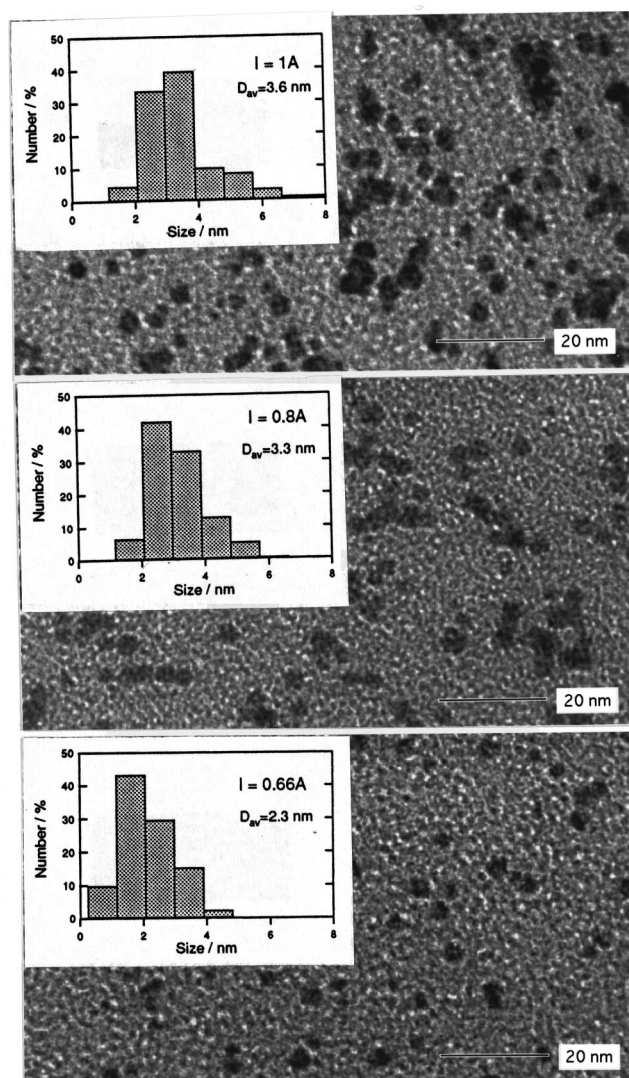


FIG. 4. Nanometer size Ni clusters observed by TEM obtained with  $V_{Ar} = 1.5 \times 10^{-4}$  and  $V_{He} = 3.0 \times 10^{-4} \text{ mol/s}$ .  $I$  is current for the sputtering source and  $D_{av}$  is an average cluster size.

$V_{He} = 0 - 7.4 \times 10^{-4} \text{ mol/s}$ . A larger amount of clusters is produced for longer  $L_g$  and larger  $V_{He}$ . It is obvious that the He gas flow effectively carries the clusters because the viscosity of He gas is lower than that of Ar gas. Figure 6 shows the TEM image sequence of Ni clusters prepared with  $L_g = 100, 120$ , and  $170 \text{ mm}$  at  $V_{Ar} = 1.5 \times 10^{-4}$  and  $V_{He} = 4.5 \times 10^{-4} \text{ mol/s}$ . The corresponding size distributions estimated within the area of  $0.034 \mu\text{m}^2$  are shown in Fig. 7. The cluster size decreases with decreasing  $L_g$  because the total amount of collisions between cluster-cluster and/or cluster-vapor atom would be proportional to the drift time,  $L_g / \nu_z$ .

Figure 8 shows the deposition rate versus  $L_g$  curves for  $V_{Ar} = 3.0 \times 10^{-4}$  and  $V_{He} = 0 - 7.4 \times 10^{-4} \text{ mol/s}$ . These curves are totally different from those for  $V_{Ar} = 1.5 \times 10^{-4} \text{ mol/s}$ . The cluster deposition is detectable even at  $L_g = 60 \text{ mm}$ . The deposition rate first increases with increasing  $L_g$  below  $100 \text{ mm}$ , but shows two peaks at around  $L_g = 100$  and  $180 \text{ mm}$ . It is also notable that the deposition monitor markedly fluctuated at  $L_g = 100$  and  $180 \text{ mm}$ . The

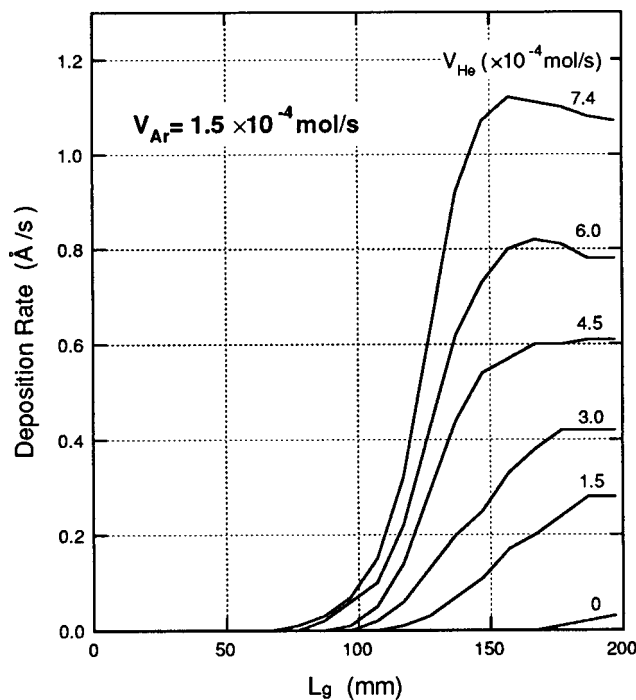


FIG. 5. Cluster deposition rate as a function of growth length,  $L_g$ , for  $V_{Ar} = 1.5 \times 10^{-4}$ ,  $V_{He} = 0 \sim 7.4 \times 10^{-4}$  mol/s, and  $I = 1$  A.

TEM images inserted in Fig. 8 show a broader distribution in the cluster size for  $L_g = 180$  mm. On the other hand, we obtained monodisperse Ni clusters for  $L_g = 80$  and 140 mm, where the deposition rate was very stable. The deposition rate fluctuation and the broad size distribution at  $L_g = 100$  and 180 mm suggest that vortical flows may be induced for the corresponding growth length and clusters cannot be transported smoothly.

## IV. DISCUSSION

### A. Embryo formation

In the PGC process, vaporized metal atoms from the target rapidly lose their kinetic energy by collisions with the inert gas atoms. The first step of the cluster growth is embryo formation by thermodynamical fluctuation through three-body collisions. This process is very difficult to analyze by a conventional collision dynamics because there are a lot of unknown factors and lack of theory. These embryos are so small that they easily evaporate instead of growing to larger clusters.<sup>14</sup>

The cluster formation strongly depends on the presence of nucleation centers such as impurity atoms, ions, etc., i.e., heterogeneous nucleation. In the PGC process, a large amount of the metal atoms are ionized by penning process,<sup>5,15</sup> where the electrons in the glow discharge region can excite Ar atoms to the metastable state of 11.5 eV, whose lifetime of 1 s is much longer than the inverse of the collision frequency. This energy level is higher than the first ionization energy of Ni atom (7.63 eV),<sup>16</sup> so that the fraction of ionized Ni atom increases, which may promote the embryo formation. This is a dynamic process with slightly pre-

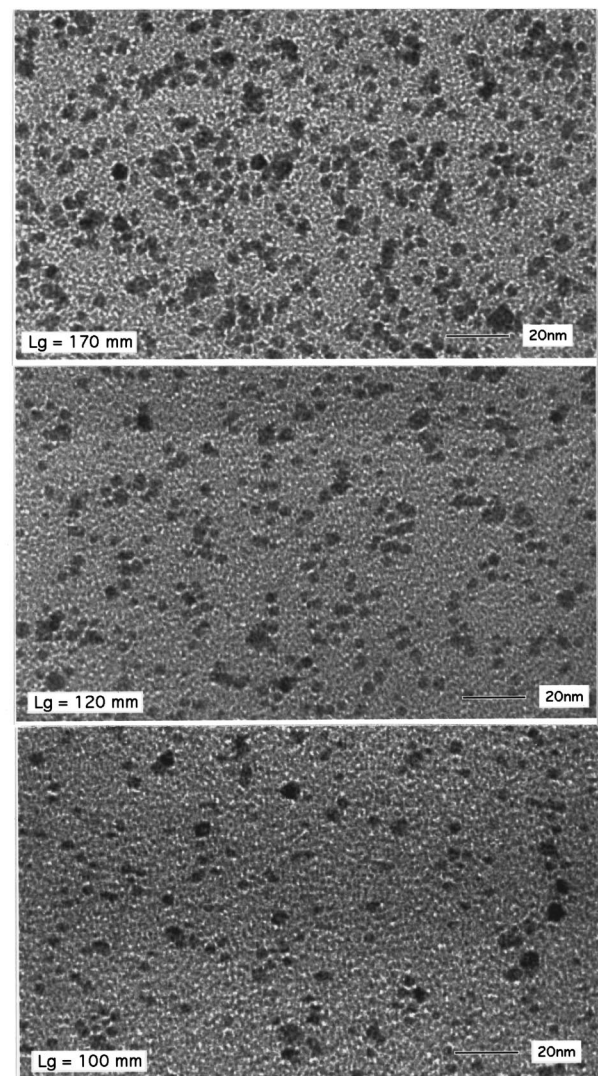


FIG. 6. TEM images of the samples prepared with varying growth length,  $L_g = 100, 120$ , and 170 mm, for  $V_{Ar} = 1.5 \times 10^{-4}$ ,  $V_{He} = 4.5 \times 10^{-4}$  mol/s, and  $I = 1$  A.

dominating condensation. In this report, however, we neglect this process and regard simply homogeneous nucleation as a first approach to the cluster growth.

When we consider the cluster growth, there are two major processes. (1) A cluster-cluster collision process: clusters react with each other, and (2) an atomic condensation process: the clusters grow with accepting atoms arrived on their surface one by one. In Secs. IV B and IV C, we try to interpret our experimental results using these concepts.

### B. Cluster-cluster collision

In order to estimate the cluster growth, we need a metal vapor density. Based upon experimental and theoretical results on sputtering,<sup>17,18</sup> the sputtering yield,  $S_y = N_s/N_i$ , is about 5 for our operating condition, where  $N_i$  is the number of incident ions onto the target and  $N_s$  that of evaporated atoms. The density of sputtered atoms from the target (80

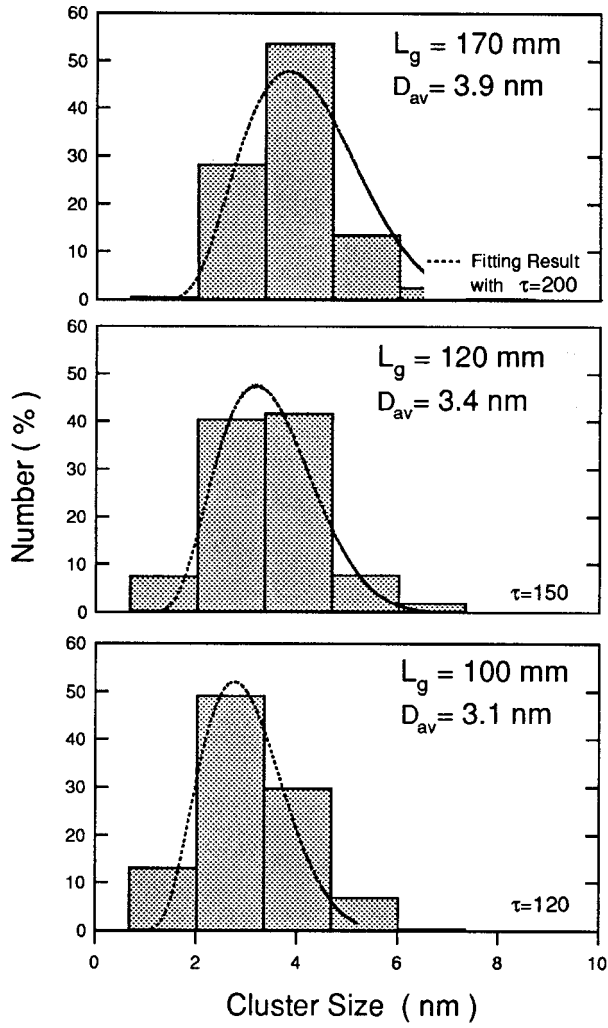


FIG. 7. Size distributions estimated from Fig. 6. Broken lines are the results of simulation based on cluster-cluster collisions with frequency  $\tau$  in Eq. (5).  $L_g$  is the growth length and  $D_{av}$  is an average cluster size.

mm in diameter) is then about  $1.6 \times 10^{19}$  atoms/m<sup>3</sup> at  $I = 1.0$  A, provided that there are only Ar ions and electrons in the initial plasma.

The supersaturation factor,  $S$ , is related with the cluster radius,  $r$ , as follows:<sup>19</sup>

$$\ln S = \ln \frac{p_r}{p_\infty} = \frac{2\Gamma V_a}{k_B T r}. \quad (3)$$

Here,  $\Gamma$  is the surface tension and  $V_a$  is the atomic volume.  $P_r$  and  $P_\infty$  are the equilibrium vapor pressure of the cluster with radius  $r$  and that of the plane surface, respectively.

The model applied for the cluster-cluster collision is simulated by assuming that the cluster grows when it collides with another, and that the total mass in the system is conserved.<sup>11</sup> We also neglect the evaporation from the cluster surface, because for large clusters,  $P_r$  becomes comparable to  $P_\infty$ . The kinetic equation for the collision process is given by the following equation similar to that for the gas atom collision.<sup>11</sup>

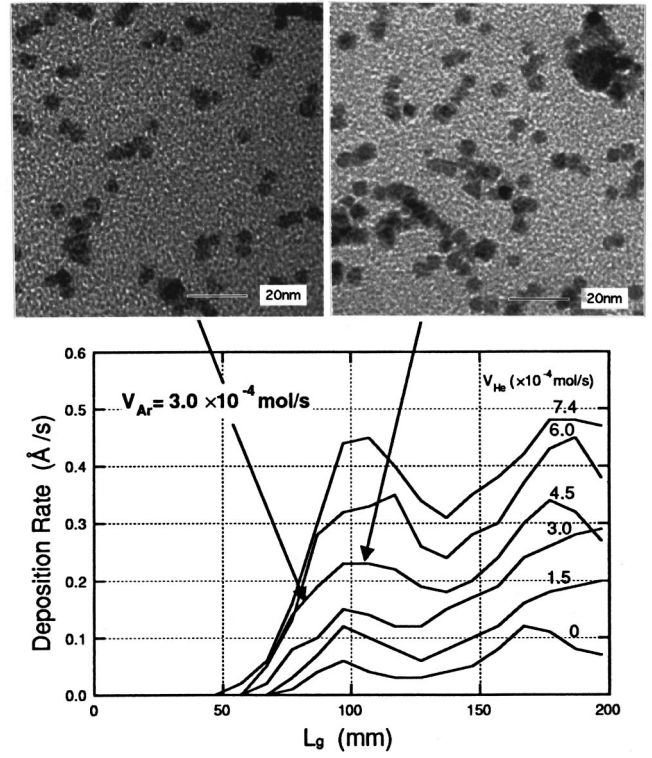


FIG. 8. Cluster deposition rate as a function of growth length,  $L_g$ , for  $V_{Ar} = 1.5 \times 10^{-4}$ ,  $V_{He} = 0 - 7.4 \times 10^{-4}$  mol/s, and  $I = 1$  A.

$$\frac{dn_k}{d\tau(t)} = \sum_{\substack{i+j=k \\ i \leq j}} C_{i,j} n_i n_j - \sum_i C_{i,k} n_i n_k, \quad (4)$$

with

$$C_{i,j} = \pi(r_i + r_j)^2 \left( \frac{8k_B T}{\pi m_*} \right)^{1/2}.$$

Here,  $n_k$  is the number of the  $k$ -size clusters per unit volume and the coefficient  $C_{i,j}$  is a product of the collision cross section by the mean speed between the  $i$ - and the  $j$ -size clusters.  $r_i = r_1 i^{1/3}$  is the radius of the  $i$ -size cluster composed of  $i$  atoms and  $m_* = m_i m_j / (m_i + m_j)$  is the reduced mass, where  $m_i$  and  $m_j$  are the masses of the  $i$ - and  $j$ -size clusters. The initial condition of  $n_k$  is  $1.6 \times 10^{19}$  for  $k = 1$ , as we estimated in the present experimental condition, and  $n_k = 0$  for  $k \neq 1$ .

This approach is based on the view that the growth rate for the  $k$ -size cluster is the total sum of the increasing number of collisions between  $i$ - and  $j$ -size clusters ( $k = i + j$ ) and the decreasing number of the  $k$ -size cluster to larger size cluster by collisions. The parameter  $\tau(t)$  is the collision frequency<sup>11,19</sup>

$$\tau(t) = \int_0^t \sqrt{2} \sigma v_{th} \frac{n(\tau)}{V} dt', \quad (5)$$

where  $\sigma$  is the cross section,  $v_{th}$  is the thermal velocity of the clusters, and  $V$  is the volume of system. Note that  $\sigma$  becomes larger when a larger cluster meets smaller clusters or vice versa, indicating that the smaller clusters disappear as soon as the larger ones are formed.

The results of this simulation are shown in Fig. 7 by the broken lines and overlap well with the size distribution estimated from the TEM results. Here, we obtained  $\tau=120$  for the average cluster size of 3.1 nm. This value corresponds to  $t=45$  s in Eq. (5), which is two orders longer than the real traveling time of 0.25 s for  $L_g=100$  mm. The cluster density decreases rapidly as clusters grow and it takes a much longer time for the cluster-cluster collision. Therefore, this collision process is not appropriate for the present results.

### C. Vapor condensation growth

We presume here that some embryos in the growth region grow into larger clusters by a two-body collision, as mentioned in Sec. I. The growth rate by adding only atoms can then be expressed as<sup>12</sup>

$$\frac{di}{dt} = \nu_z \frac{di}{dz} = \sigma_{a,i} \nu_{th} n_0 (1 - \eta), \quad (6)$$

where  $i$  is the cluster size,  $\nu_z$  is the drift velocity of the materials as we estimated from the flow rate, and  $n_0$  is the vapor density.  $\eta$  is a reevaporation to condensation rate factor, which consider the evaporation from the cluster surface. Note that  $\eta$  can be close to 1 if the cluster is small, i.e., the reevaporation rate,  $\phi_r$ , is comparable to the condensation rate,  $\phi_c$ , because the latent heat of condensation of metals is large, e.g., 4.4 eV for Ni at 0 K and 1 atm.  $\nu_{th}$  is the mean velocity with the reduced mass of the  $i$ -size clusters,  $m_i$ , and the vapor atom,  $m_a$ ,  $m_* = m_i m_a / (m_i + m_a)$ , and  $\sigma_{a,i}$  is the collision cross section between them<sup>19</sup>

$$\nu_{th} = \left( \frac{8k_B T}{\pi m_*} \right)^{1/2}, \quad \sigma_{a,i} = \pi (r_a + r_i)^2, \quad (7)$$

where  $r_a$  and  $r_i$  are the radii of the vapor atom and the  $i$ -size cluster.

A practical problem to solve the differential equation of Eq. (6) is the estimation of  $\eta$ . A heat flow between the cluster and vapor has been discussed by Knauer<sup>12</sup> for the case of an adiabatic expansion. In his argument, the rate of heat delivery from vapor to cluster and from cluster to vapor should be equal during the cluster growth. For the PGC process, however, the latent heat can be removed by collisions with high dense inert gas atoms, i.e., the clusters are not adiabatically cooled down. A simple explanation for  $\eta$  can be possible because vaporization is generally proportional to the vapor pressure:<sup>19</sup>  $\phi_r$  is proportional to the vapor pressure above a cluster surface with radius  $r$ ,  $P_r$ , [see Eq. (3)] and  $\phi_c$  is commensurate to that of material atoms around the clusters,  $P_v$

$$\eta \propto \frac{\phi_r}{\phi_c} = \frac{P_\infty}{P_v} \exp \left( \frac{2\Gamma V_a}{k_B T r_i} \right). \quad (8)$$

The main assumption here is that the density of vaporized metal atoms does not decrease with the cluster growth, i.e., the density of the cluster nucleus is low enough, so that they do not markedly consume the vaporized metal atoms for their growth. Equation (6) can then be solved numerically by setting the initial cluster size,  $i_0$ . As we mentioned before, the embryo size would be about 7 by Monte Carlo

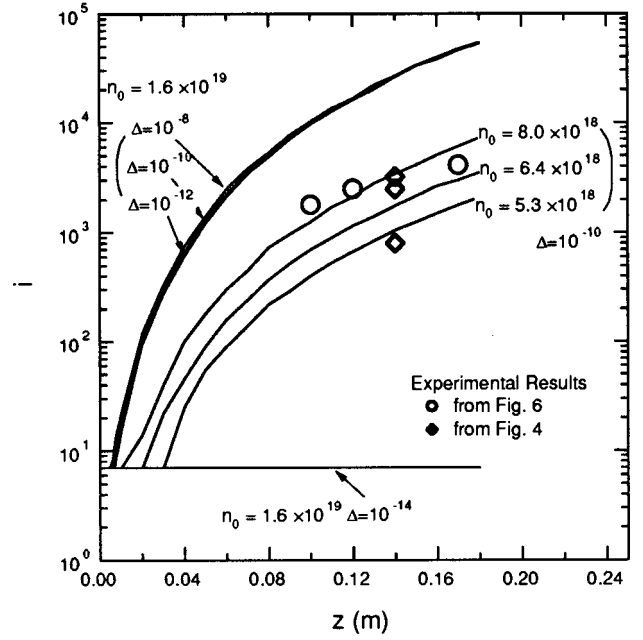


FIG. 9. Cluster size,  $i$ , dependence on its traveling length,  $z$ , obtained from numerical solution of differential equation (9).  $n_0$  is a vapor density of metal atoms and  $\Delta$  is a fluctuation value of the initial cluster size,  $i'_0 = 7 + \Delta$ .

simulation.<sup>10</sup> Normalizing Eq. (8) by the initial pressure ratio of the  $i_0$ -size cluster to vaporized metal atoms, we obtain the following equation:

$$\frac{di}{dz} = \frac{\pi r_a^2 i^{2/3} n_0}{\nu_z} \left( \frac{8k_B T}{\pi m_a} \right)^{1/2} \{1 - \exp[2\Gamma V_a \theta / (k_B T r_a)]\} \quad (9)$$

with

$$\theta = (i_0^{1/3} - i^{1/3}) / i_0^{1/3} i^{1/3},$$

where  $m_a$  is the mass of the vaporized metal atom. The following approximations are also adopted:

$$\frac{1}{m_*} = \frac{1}{m_a} + \frac{1}{m_i} \approx \frac{1}{m_a}; \quad r_i + r_a \approx r_i = r_a i^{1/3}. \quad (10)$$

This differential equation is unstable at the start point,  $i=i_0$ , because  $\phi_r = \phi_c$ , i.e., the embryo can never grow to a larger cluster. The cluster can, however, become larger by arriving adatom on the surface if the numerical solution is started from an  $i'_0$  value which is slightly larger than the embryo size, i.e.,  $i'_0 = i_0 + \Delta$ , where  $0 < \Delta \ll 1$ .

The solutions of Eq. (8) as a function of the traveling length,  $z$ , corresponding to  $L_g$  in the present experiment are shown in Fig. 9 with different  $\Delta$  values for  $i_0=7$  ( $r_a=1.24$  Å,  $M_a=9.7 \times 10^{-26}$  kg,  $\Gamma=1.7$  N/m,  $T=300$  K). The experimental results obtained in the present work (see Figs. 4 and 6) are also indicated. The experimental cluster size at different  $L_g$ 's is overlapped well with the solution lines estimated for  $n_0=8 \times 10^{18}$ . The reduction in their size by decreasing the sputtering power is also consistent with the numerical solutions for smaller  $n_0$  values ( $6.4 \times 10^{18}$  and  $5.3 \times 10^{18}$ ). One can see that, when  $\Delta=10^{-14}$ , an embryo cannot grow. If  $\Delta$  is larger than  $10^{-14}$ , however, it grows and

the variation of  $\Delta$  value does not conspicuously influence the final cluster size. This result indicates that clusters practically grow from embryos. When the embryo is stabilized by chance, the condensation starts: the cluster growth rate increases by increasing their size because the evaporation from the cluster surface rapidly decreases.

#### IV. CONCLUSION

We have constructed a plasma-gas-condensation type cluster deposition apparatus. The small clusters of about 2 nm in diameter were obtained with the low sputtering power and the small volume of the cluster growth region. We applied two models for the cluster growth; cluster-cluster collision and vapor condensation processes. In the cluster-cluster collision process, the collision frequency decreases as the cluster size becomes larger. The clusters cannot grow as fast as the experimental results, even though the size distributions observed by TEM are well fitted by the cluster-cluster collision simulation. The atomic vapor condensation process, on the other hand, gives a reasonable explanation for the real cluster growth. The atoms evaporate easily from the embryo surface. However, it can grow to a larger cluster, when its free energy is decreased accidentally by fluctuation. The final size of the clusters are as large as that obtained by TEM observations.

#### ACKNOWLEDGMENTS

The authors wish to thank Dr. T. J. Konno for the support of the TEM observation, Dr. M. Sakurai for helpful suggestions, and Dr. S. Yamamuro for useful comments. They gratefully acknowledge technical contributions to the PGC cluster deposition apparatus from Viotech Japan Co.,

Ltd. They are also indebted to the Laboratory for Developmental Research of Advanced Materials, Institute for Materials Research, Tohoku University. This work was supported by CREST (Core Research for Evolutional Science and Technology) of Japan Science and Technology Corporation (JST).

- <sup>1</sup>W. A. de Heer, Rev. Mod. Phys. **65**, 611 (1993).
- <sup>2</sup>P. Melinon *et al.*, Int. J. Mod. Phys. B **9**, 339 (1995).
- <sup>3</sup>H. Haberland, in *Clusters of Atoms and Molecules I*, edited by H. Haberland (Springer, Berlin, 1995), p. 207.
- <sup>4</sup>S. Yatsuya, T. Kamakura, K. Yamauchi, and K. Mihama, Jpn. J. Appl. Phys., Part 2 **25**, L42 (1986).
- <sup>5</sup>H. Haberland, M. Karrais, M. Mall, and Y. Thurner, J. Vac. Sci. Technol. A **10**, 3266 (1992).
- <sup>6</sup>G. Hohl, T. Hihara, M. Sakurai, T. Oishi, K. Wakoh, K. Sumiyama, and K. Suzuki, Jpn. J. Appl. Phys., Part 1 **33**, 1509 (1994).
- <sup>7</sup>S. Yamamuro, M. Sakurai, T. J. Konno, K. Sumiyama, and K. Suzuki, in *Similarities and Differences Between Atomic Nuclei and Clusters*, edited by Y. Abe *et al.* [AIP Conf. Proc. **416**, 491 (1997)].
- <sup>8</sup>S. Yamamuro, K. Sumiyama, M. Sakurai, and K. Suzuki, Supramol. Sci. (in press).
- <sup>9</sup>C. G. Granqvist and R. A. Buhrman, J. Appl. Phys. **47**, 2200 (1976).
- <sup>10</sup>M. Kappes and S. Leutwyler, in *Molecular Beams of Clusters in Atomic and Molecular Beam Methods*, edited by G. Scoles (Oxford University Press, New York, 1988), Vol. 1, p. 380.
- <sup>11</sup>J. M. Soler, N. García, O. Echt, K. Sattler, and E. Recknagel, Phys. Rev. Lett. **49**, 1857 (1982).
- <sup>12</sup>W. Knauer, J. Appl. Phys. **62**, 841 (1987).
- <sup>13</sup>O. F. Hagen, Surf. Sci. **106**, 101 (1981).
- <sup>14</sup>A. Milchev and J. Malinowski, Surf. Sci. **156**, 36 (1985).
- <sup>15</sup>B. Chapman, *Glow Discharge Processes* (Wiley, New York, 1982).
- <sup>16</sup>H. Haken and H. Wolf, *The Physics of Atoms and Quanta* (Springer, New York, 1996).
- <sup>17</sup>J. L. Vossen and W. Kern, *Thin Film Processes* (Academic, New York, 1978).
- <sup>18</sup>P. Sigmund, Phys. Rev. Lett. **184**, 383 (1969).
- <sup>19</sup>P. W. Atkins, *Physical Chemistry* (Oxford University Press, New York, 1995).